

Quantum-inspired search method for low-energy states of classical Ising Hamiltonians

Hiroshi Ueda^{1,2} and Seiji Yunoki^{1,3,4}

¹*Computational Materials Science Research Team,*

RIKEN Center for Computational Science (R-CCS), Kobe 650-0047, Japan

²*JST, PRESTO, Kawaguchi, 332-0012, Japan*

³*Computational Condensed Matter Physics Laboratory,*

RIKEN Cluster for Pioneering Research (CPR), Wako, Saitama 351-0198, Japan and

⁴*Computational Quantum Matter Research Team,*

RIKEN Center for Emergent Matter Science (CEMS), Wako, Saitama 351-0198, Japan

(Dated: October 2, 2020)

We develop a quantum-inspired numerical procedure for searching low-energy states of a classical Hamiltonian including two-body full-connected random Ising interactions and a random local longitudinal magnetic field. In this method, we introduce infinitesimal quantum interactions that cannot commute with the original Ising Hamiltonian, and generate and truncate direct product states inspired by the Krylov subspace method to obtain the low-energy spectrum of the original classical Ising Hamiltonian. The numerical cost is controllable by the form of infinitesimal quantum interactions, the number I of numerical iterations, the number L of initial classical states, and the number K of states kept. To demonstrate the method, here we introduce as the infinitesimal quantum interactions pair products of Pauli X operators and on-site Pauli X operators into the random Ising Hamiltonian, for which the numerical cost is $O(N^3)$ per a numerical iteration with the system size N . We consider 120 instances of the random coupling realizations for the random Ising Hamiltonian in each N up to 30 and perform the calculations to search the 120 lowest-energy states of each Hamiltonian. We show that the procedure with $(L, K, I) = (N, N(N+1)/2 + 1, N)$ finds all the ground states successfully and about 99% of the 120 lowest-energy states.

I. INTRODUCTION

Combinatorial optimization problems, which are classified in the NP-complete or NP-hard problem (NP problem), can be mapped to the ground-state search problem of a classical Ising model [1]. The classical Ising model for N -site systems can be written as

$$\hat{H}_0 = \sum_{i<j} J_{ij} \hat{\sigma}_i^z \hat{\sigma}_j^z + \sum_i h_i \hat{\sigma}_i^z, \quad (1)$$

where $\hat{\sigma}_i^z$ is a Pauli- Z operator for the i th site. The search of the ground states of the Ising model with general J_{ij} , which is referred to as the spin glass model, is known to be categorized in an NP problem [2–4]. A traditional numerical approach for the search of the ground state is the simulated annealing [5] by use of the thermal fluctuation.

A quantum analogy of the annealing process is employed in the quantum annealing [6–10], which is a kind of a quantum adiabatic optimization approach. In the quantum annealing, we adopt an additional Hamiltonian \hat{H}_1 , whose ground state is easily found numerically or experimentally, with $[\hat{H}_0, \hat{H}_1] \neq 0$. Then, we introduce a time-dependent Hamiltonian

$$\hat{H}(t) = \left(1 - \frac{t}{t_0}\right) \hat{H}_1 + \frac{t}{t_0} \hat{H}_0, \quad (2)$$

and perform the real-time evolution $|\Psi(t)\rangle = T \left[\exp\left[\frac{i}{\hbar} \int_0^t \hat{H}(t') dt'\right] |\Psi(0)\rangle \right]$ with the ground state $|\Psi(0)\rangle$ of \hat{H}_1 and the T-product $T[\cdot]$. If t_0 is large enough and there is no level crossing between the ground state and excited states of $\hat{H}(t)$ for all the time during the process, $|\Psi(t)\rangle$ follows the ground state of

the instantaneous Hamiltonian $\hat{H}(t)$ and eventually evolves into the ground state of \hat{H}_0 at $t = t_0$ by the adiabatic theorem for quantum systems [11–14]. When $\hat{H}(t)$ undergoes a first-order phase transition during the process at $0 < t < t_0$ in the thermodynamic limit, the quantum annealing does not work unless one introduces an additional quantum Hamiltonian to avoid the transition [15, 16].

These classical and quantum annealing approaches are overall satisfactory to search the ground state of the Hamiltonian \hat{H}_0 , which in turn can solve a combinatorial optimization problem for the practical social applications if the mappings to \hat{H}_0 are flawless. However, the perfect mapping is known to be generally a difficult task. Even when the mappings are not exactly perfect, we still expect that the solution that matches the needs for the practical social problem can still be found in one of the low-energy excited states of the mapped Hamiltonian \hat{H}_0 . A Monte Carlo method such as the histogram reweighting techniques [17, 18] and the Wang-Landau sampling [19] might be a good candidate for solving such a problem. Indeed, these methods can efficiently evaluate the density of states of a classical Ising model in a wide range of energy. However, they are not suitable for accurately determining the sequence of lowest-energy states, for example, the lowest 100 excited states from the ground state. Therefore, it is highly desirable to develop a solver for the search of the low-energy states of \hat{H}_0 with computational complexity of $O(\text{poly}(N))$.

In this paper, we develop a quantum-inspired algorithm for searching the low-energy states of the classical Ising Hamiltonian \hat{H}_0 in Eq. (1) with random couplings J_{ij} and h_i . In this algorithm, we introduce infinitesimal quantum interactions \hat{H}_1 as in the case of the

quantum annealing, and generate and truncate classical direct product states inspired by the Krylov subspace method [20], which is a successful method available in the numerical linear algebra, to obtain the low-energy states of \hat{H}_0 . The numerical and physical memory costs of the algorithm are controllable by the form of \hat{H}_1 , the number I of numerical iterations, the number L of initial classical states, and the number K of states kept. For the demonstration of our method, we introduce all possible pair products of Pauli X operators and on-site Pauli X operators as \hat{H}_1 , for which the numerical cost is $O(N^3)$ per an iteration with the system size N . We consider 120 different instances of the random coupling J_{ij} and h_i realizations in each system size N up to 30 sites and perform the calculations to obtain the 120 lowest-energy states. We show that our algorithm with $(L, K, I) = (N, N(N+1)/2 + 1, N)$ finds the ground state successfully and about 99% of the 120 lowest-energy states for each instance of the random couplings in \hat{H}_0 .

The rest of this paper is organized as follows. In Sec. II, we first summarize the basic physical properties of the classical Ising model described by the Hamiltonian \hat{H}_0 in Eq. (1) that are obtained by the brute-force numerical search over all spin configurations. Then, we describe our quantum-inspired algorithm for the search of low-energy states of \hat{H}_0 in Sec. III. As the benchmark calculations, we analyze the efficiency of our algorithm for searching the 120 lowest-energy states, including the ground state, of \hat{H}_0 in Sec. IV. The summary and conclusion are provided in Sec. V.

II. BASIC PHYSICAL PROPERTY OF \hat{H}_0

In this study, we consider the classical Ising model described by the Hamiltonian \hat{H}_0 in Eq. (1) with the fully connected random interactions J_{ij} and the random magnetic fields h_i that are both uniformly distributed in the range of $[-1/2, 1/2]$. Here, we first investigate this classical Ising model by the brute-force numerical search over all spin configurations and summarize the basic physical properties such as the ground state energy, the first excitation gap, and the number of state in the thermodynamic limit that are ensemble averaged over the different random coupling realizations. Note that the Hamiltonian \hat{H}_0 with the couplings (J_{ij}, h_i) replaced with $(J_{ij}/\sqrt{N}, 0)$ and J_{ij} being distributed according to the Gaussian distribution is well known as the Sherrington-Kirkpatrick (SK) model [21], and the ground state of the SK model has been studied by various numerical methods such as genetic algorithms [22, 23], hierarchical methods [24], extremal optimizations [25], and conformational space annealing [26].

To evaluate the physical quantities, we consider 120 instances of the random coupling realizations in \hat{H}_0 for each system size N up to 30 sites, which are treated by the brute-force numerical search with reasonable computational time. Figures 1(a) and 1(b) show the ensemble-averaged ground state energy and the ensemble-averaged

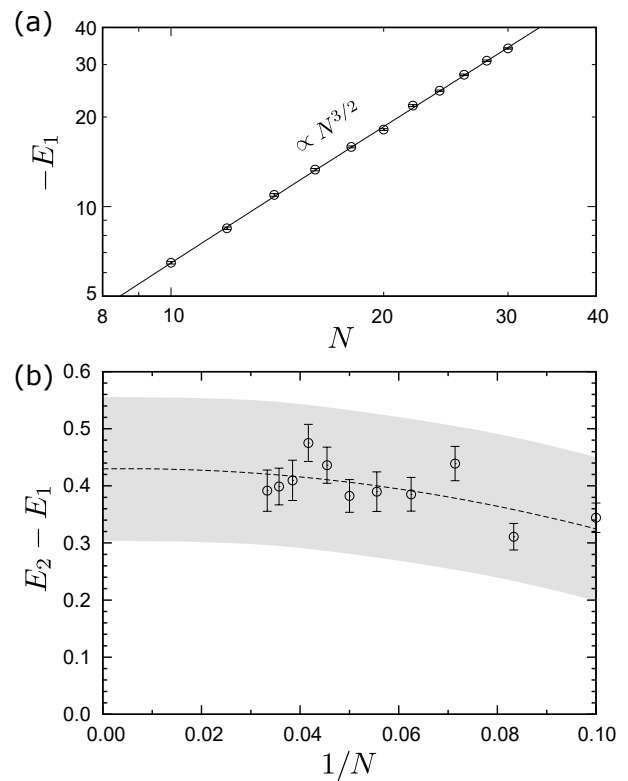


FIG. 1. (a) Ensemble-averaged ground-state energy E_1 as a function of the system size N . Solid line is the fitting function $E_1 = aN^{3/2} + b$ with $a = -2.09 \pm 0.02$ and $b = 0.15 \pm 0.11$. (b) Ensemble-averaged first excitation gap $E_2 - E_1$ as a function of $1/N$. The dashed line is the quadratic-fit for the gap and the grey shade indicates the fitting error in the thermodynamics limit, i.e., $1/N \rightarrow 0$.

first-excited energy, respectively, plotted as a function of the system size N and its inverse $1/N$. In these figures, the error bars indicate the standard error due to the ensemble average over the 120 random coupling realizations. As shown in Fig. 1(a), we find the ensemble-averaged ground state energy E_1 is clearly proportional to $N^{3/2}$ and it is well fitted by a function $E_1 = aN^{3/2} + b$ with $a = -2.09 \pm 0.02$ and $b = 0.15 \pm 0.11$, where the error bars are the standard error due to the fit. Note that the reading exponent $N^{3/2}$ is exactly the same as that of the SK model [21], considering that the random coupling in the SK model is scaled with N as J_{ij}/\sqrt{N} . To estimate the first excitation gap in the thermodynamic limit, we perform a quadratic fit of the ensemble-averaged first excited energy $E_2 - E_1$ with respect to $1/N$ as shown in Fig. 1(b), and find that there exists a finite gap in the thermodynamic limit as $E_2 - E_1 = 0.42 \pm 0.12$.

We also investigate the total number of states $k(E)$ below a certain energy E in the low-energy region because the first derivative of $k(E)$ with respect to E corresponds to the density of states at energy E . For this purpose, here we simply calculate the k th lowest energy E_k that is ensemble averaged over the 120 different random coupling realizations. Figure 2(a) shows the

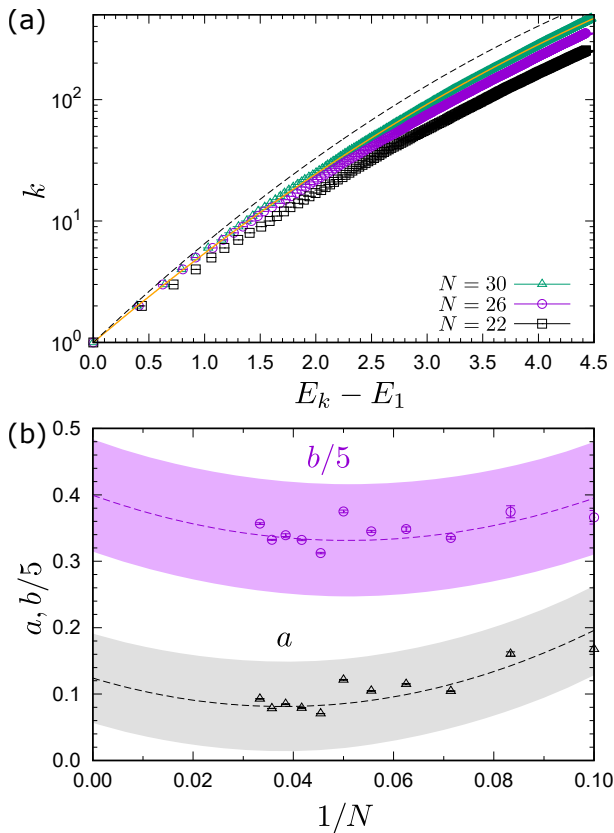


FIG. 2. (Color online) (a) Ensemble-averaged energy difference $E_k - E_1$ between the k th lowest energy and the ground state energy over the 120 different random coupling realizations in \hat{H}_0 for the system size $N = 22, 26$, and 30 sites. The orange line is the fitting function $\ln k = -a(E_k - E_1)^2 + b(E_k - E_1)$ with $a = 0.0927(3)$ and $b = 1.783(2)$ for the data of $N = 30$. The black dashed line is the fitting function in the thermodynamic limit with $(a, b) = (0.12, 2.0)$ estimated in (b). (b) Fitting parameters a and b as a function of $1/N$. These parameters are obtained by fitting the results of k vs. $E_k - E_1$ for each system size N , as in (a). The purple and black dashed lines are the quadratic fits for these parameters a and b , respectively. The purple and gray shades indicate the fitting errors of a and b , respectively, in the thermodynamic limit, i.e., $1/N \rightarrow 0$.

semi-log plot of k vs. $E_k - E_1$ in the low-energy region for $N = 22, 26$, and 30 sites. Here, $E_1 - E_k$ corresponds to the ensemble-averaged energy difference between k th lowest energy and the ground state energy. We find that $\ln k$ is almost proportional to $E_k - E_1$ in the lowest-excited energy region $E_k - E_1 \sim 0$ and gradually shifts to an upward-convex function with increasing $E_k - E_1$. As a phenomenological fitting function, we propose $\ln k = -a(E_k - E_1)^2 + b(E_k - E_1)$ with positive fitting parameters a and b . Applying the least-square fitting to the data for $N = 30$, we obtain the fitting curve with $a = 0.0927(3)$ and $b = 1.783(2)$ that is indicated by the orange line in Fig. 2(a), confirming that the fitting curve well fits the data for $E_k - E_1 \leq 4.5$.

Next, we estimate the fitting curve in the thermody-

amic limit by first fitting the data of k vs. $E_k - E_1$ for each system size N to obtain a and b as a functions of $1/N$. Then we perform quadratic fittings of a and b with respect to $1/N$ and estimate the parameters a and b in the thermodynamic limit by extrapolating them to $1/N \rightarrow 0$, as shown in Fig. 2(b). The fitting curve with a and b in the thermodynamic limit is indicated by the black dashed line in Fig. 2(a), which is comparable with the data for $N = 30$ in the region of $E_k - E_1 \lesssim 1$. Notice also that the first-excited energy $E_2 - E_1$ is almost on the dashed line, thus consistent with the results shown in Fig. 1(b).

III. ALGORITHM

In this section, we describe algorithms composing our quantum-inspired (QI) search algorithm proposed in this paper. First, we introduce $|\sigma\rangle \in \{|0\rangle, |1\rangle\}$ as a complete set of a local qubit, which are eigenstates of the Pauli-Z operator, i.e., $\hat{\sigma}^z |0\rangle = |0\rangle$ and $\hat{\sigma}^z |1\rangle = -|1\rangle$. Using this local basis set, we can express any state for a N -qubit system as $|\sigma\rangle = (\sigma_0, \dots, \sigma_{N-1})$, which forms the complete set of states. For the fast simulation in the classical computer, we employ a typical form of the state list that makes a one-to-one correspondence between the vector σ and an integer ψ representing a state as follows:

$$|\psi\rangle \equiv |\sigma\rangle \text{ with } \psi = (\sigma_{N-1} \dots \sigma_1 \sigma_0)_2 = \sum_{i=0}^{N-1} 2^i \sigma_i. \quad (3)$$

Next, as an basic operation in the search algorithm, we define a procedure to obtain the ℓ -site spin-flipped state $|\psi'\rangle = \prod_{k=1}^{\ell} \hat{\sigma}_{i_k}^x |\psi\rangle$ for a given state $|\psi\rangle$ with $1 \leq \ell \leq N$ and $0 \leq i_1 < \dots < i_\ell < N$. Here, $\hat{\sigma}_i^x$ is the Pauli-X operator acting at the i th site. For this operation, we often employ the bitwise exclusive or operation (BITXOR), as shown in Algorithm 1.

Algorithm 1 Multiple Spin flip for N -site systems

Input: integer ψ in Eq. (3), ℓ with $1 \leq \ell \leq N$, and $\mathbf{i} = (i_1, \dots, i_\ell)$ with $0 \leq i_1 < \dots < i_\ell < N$.
Output: integer ψ' with $0 \leq \psi' < 2^N$.
1: **function** MULTIPLE_SPIN_FLIP(ψ, \mathbf{i}, ℓ)
2: $x := \sum_{k=1}^{\ell} 2^{i_k}$
3: $\psi' := \text{BITXOR}(x, \psi)$
4: **end function**

The core function for the update of state lists in our search algorithm is shown in Algorithm 2. Now, it is assumed that we have already kept the $(K+1)$ -dimensional integer vector ψ and the $(K+1)$ -dimensional real vector \mathbf{E} for specifying $K+1$ classical product states $\{|\psi_i\rangle\}$ and the corresponding energies $\{E_i = \langle \psi_i | \hat{H}_0 | \psi_i \rangle\}$, where the order of integers $\psi_1, \psi_2, \dots, \psi_{K+1}$ has already been sorted so that $E_1 \leq E_2 \leq \dots \leq E_{K+1}$. It is also assumed that we have already kept the $(K+1)$ -dimensional logical

Algorithm 2 Update list of states

Input: integer ψ , ℓ , \mathbf{i} , K with $1 \leq K < 2^N$, $\boldsymbol{\psi} = \{\psi_i\}_{1 \leq i \leq K+1}$, and $\boldsymbol{\psi}' = \{\psi'_i\}_{1 \leq i \leq K+1}$ with $0 \leq \psi'_1 < \dots < \psi'_{K+1} < 2^N$; real $\mathbf{E} = \{\langle \psi_i | \hat{H}_0 | \psi_i \rangle\}_{1 \leq i \leq K+1}$ with $E_1 \leq \dots \leq E_{K+1}$; logical variable $\mathbf{l} = \{l_i\}_{1 \leq i \leq K+1}$

Output: integer $\boldsymbol{\psi}$ and $\boldsymbol{\psi}'$; real \mathbf{E} ; logical variable \mathbf{l}

- 1: **function** UPDATE_LIST($\psi, \mathbf{i}, \ell, \boldsymbol{\psi}, \boldsymbol{\psi}', \mathbf{E}, \mathbf{l}, K$)
- 2: $\boldsymbol{\psi}' := \text{MULTIPLE_SPIN_FLIP}(\boldsymbol{\psi}, \mathbf{i}, \ell)$
- 3: $(p, f) := \text{BINARY_SEARCH}(\boldsymbol{\psi}', \boldsymbol{\psi}', K)$

▷ The

function “BINARY_SEARCH(x, \boldsymbol{x}, K)” with an integer/real number x and a $(K + 1)$ -dimensional ascending-ordered integer/real vector \boldsymbol{x} returns an integer p for $x_p \leq x < x_{p+1}$ and a logical variable f which becomes True when $x_p = x$.

- 4: **if** $f = \text{False}$ **then**
- 5: $E := \langle \boldsymbol{\psi}' | \hat{H}_0 | \boldsymbol{\psi}' \rangle$
- 6: $(\boldsymbol{\psi}, \boldsymbol{\psi}', \mathbf{E}, \mathbf{l}) := \text{UPDATE_LIST_SUB}(\boldsymbol{\psi}', E, \text{False}, p, \boldsymbol{\psi}, \boldsymbol{\psi}', \mathbf{E}, \mathbf{l}, K)$
- 7: **end if**
- 8: **end function**

- 9: **function** UPDATE_LIST_SUB($\boldsymbol{\psi}', E, \ell, p', \boldsymbol{\psi}, \boldsymbol{\psi}', \mathbf{E}, \mathbf{l}, K$)
- 10: **if** $E < E_{K+1}$ **then**
- 11: $(p, f) := \text{BINARY_SEARCH}(\boldsymbol{\psi}_{K+1}, \boldsymbol{\psi}', K)$
- 12: **if** $p > p'$ **then**
- 13: $\boldsymbol{\psi}' = (\psi'_1, \dots, \psi'_{p'}, \boldsymbol{\psi}, \psi'_{p'+1}, \dots, \psi'_{p-1}, \psi'_{p+1}, \dots, \psi'_{K+1})$
- 14: **else**
- 15: $\boldsymbol{\psi}' = (\psi'_1, \dots, \psi'_{p-1}, \boldsymbol{\psi}, \psi'_{p+1}, \dots, \psi'_{p'}, \boldsymbol{\psi}, \psi'_{p'+1}, \dots, \psi'_{K+1})$
- 16: **end if**
- 17: $(p, f) := \text{BINARY_SEARCH}(E, \mathbf{E}, K)$
- 18: $\mathbf{E} := (E_1, \dots, E_p, E, E_{p+1}, \dots, E_K)$
- 19: $\boldsymbol{\psi} := (\psi_1, \dots, \psi_p, \boldsymbol{\psi}', \psi_{p+1}, \dots, \psi_K)$
- 20: $\mathbf{l} := (l_1, \dots, l_p, \mathbf{l}, l_{p+1}, \dots, l_K)$
- 21: **end if**
- 22: **end function**

vector $\mathbf{l} = \{l_i\}$ with $l_i \in \{\text{True}, \text{False}\}$ to judge whether ψ_i has already been used as an input for Algorithm 2. In addition, for the binary search of a state, we also have the $(K + 1)$ -dimensional integer vector $\boldsymbol{\psi}'$ whose elements are those of $\boldsymbol{\psi}$ but are sorted in ascending order. In Algorithm 2, we input a state $|\psi\rangle$ as the starting point and perform spin flips to generate other state $|\boldsymbol{\psi}'\rangle$. If $|\boldsymbol{\psi}'\rangle \notin \boldsymbol{\psi}'$ and the energy $E = \langle \boldsymbol{\psi}' | \hat{H}_0 | \boldsymbol{\psi}' \rangle$ is smaller than E_{K+1} , then we update the lists $\boldsymbol{\psi}$, $\boldsymbol{\psi}'$, \mathbf{l} , and \mathbf{E} by discarding $|\psi_{K+1}\rangle$ and E_{K+1} .

Having described Algorithm 2 for updating the state lists, the main algorithm of our QI single search method is finally given in Algorithm 3. For performing this algorithm, we have to prepare the set of integers \mathcal{I} for specifying the spin flip operations considered in \hat{H}_1 . For example, when \hat{H}_1 contains all patterns of J -spin flips up to $J = 2$, we set the input parameters as follows: $n_1 = N$, $\mathbf{I}_1 = \{\mathbf{i}_1^{(1)} = (0), \mathbf{i}_2^{(1)} = (1), \dots, \mathbf{i}_{N-1}^{(1)} = (N-1)\}$, $n_2 = N(N-1)/2$, and $\mathbf{I}_2 = \{\mathbf{i}_1^{(2)} = (0, 1), \mathbf{i}_2^{(2)} =$

Algorithm 3 Quantum-inspired (QI) single search method

Input: integer $N > 0$, ψ , $J > 0$, $K, I > 0$, $\mathbf{n} = \{n_j\}_{1 \leq j \leq J}$ with all $n_j > 0$, and a set of $\mathcal{I} = \{\mathbf{I}_j\}_{1 \leq j \leq J}$ where $\mathbf{I}_j = \{\mathbf{i}_n^{(j)}\}_{1 \leq n \leq n_j}$ with j -dimensional ascending-ordered integer vector $\mathbf{i}_n^{(j)}$

Output: integer $\boldsymbol{\psi}$ and $\boldsymbol{\psi}'$; real \mathbf{E} ; logical variable \mathbf{l}

- 1: **function** QI_SEARCH($N, \psi, J, K, I, \mathbf{n}, \mathcal{I}$)
- ▷ I_M/R_M : The maximum integer/real that can be expressed in a computer.
- 2: $E := \langle \psi | \hat{H}_0 | \psi \rangle$
- 3: $\boldsymbol{\psi} = \{\psi_i\}_{1 \leq i \leq K+1}$; $\psi_i := \begin{cases} \psi & i = 1 \\ I_M & \text{otherwise} \end{cases}$
- 4: $\mathbf{E} = \{E_i\}_{1 \leq i \leq K+1}$; $E_i := \begin{cases} E & i = 1 \\ R_M & \text{otherwise} \end{cases}$
- 5: $\boldsymbol{\psi}' := \boldsymbol{\psi}$
- 6: $\mathbf{l} = \{l_i\}_{1 \leq i \leq K+1}$; $\{l_i\} := \text{False}$
- 7: **for** $i = 1$ to I **do**
- 8: $f := \text{False}$
- 9: **for** $k = 1$ to $K + 1$ **do**
- 10: **if** $l_k = \text{False}$ **then**
- 11: $\psi := \psi_k$; $l_k := \text{True}$; $f := \text{True}$; **Exit**
- 12: **end if**
- 13: **end for**
- 14: **if** $f = \text{True}$ **then**
- 15: **for** $j = 1$ to J **do**
- 16: **for** $n = 1$ to n_j **do**
- 17: $(\boldsymbol{\psi}, \boldsymbol{\psi}', \mathbf{E}, \mathbf{l}) := \text{UPDATE_LIST}(\boldsymbol{\psi}, \mathbf{i}_n^{(j)}, j, \boldsymbol{\psi}, \boldsymbol{\psi}', \mathbf{E}, \mathbf{l}, K)$
- 18: **end for**
- 19: **end for**
- 20: **end if**
- 21: **end for**
- 22: **end function**

$(0, 2) \dots, \mathbf{i}_{n_2}^{(2)} = (N-2, N-1)\}$. We also input the number K of states kept, the number I of iterations, and ψ for specifying the initial classical state of the calculation.

As we shall discuss in the next section, the QI single search method is accidentally trapped in a local minimum, depending on the combination of the initial state ψ and the random coupling realization in \hat{H}_0 . One of the simplest solutions to avoid trapping in a local minimum is to perform the independent QI single searches in parallel for different random initial states and merge the lists from the independent searches. The QI multi search method shown in Algorithm 4 is based on this strategy.

Finally, we consider the computational complexity of our algorithm in Algorithm 4. The total number of the spin flip operations required per an iteration is $\sum_j n_j \sim O(N^J)$. For a spin-flipped classical state, we have to evaluate the energy of \hat{H}_0 , which costs naively $O(N^2)$. However, since we know the energy of the state before the spin flip operation, the computational cost for evaluating the energy of the state after the spin flip operation is reduced to $O(N)$ because we only take into account the couplings associated with the spin-flipped sites. The computational cost for searching a state via the binary search is $\log_2 K$

Algorithm 4 QI multi search method

Input: integer $L > 0$, N , J , K , I , \mathbf{n} , and \mathcal{I}
Output: integer ψ ; real \mathbf{E}

```

1: function QI_MULTISEARCH( $L, N, J, K, I, \mathbf{n}, \mathcal{I}$ )
2:    $\phi = \{\phi_i\}_{1 \leq i \leq L}$ ;  $\phi_i := \text{RAND\_BETWEEN}(0, 2^N - 1)$ 
    $\triangleright$  The function  $\text{RAND\_BETWEEN}(a, b)$  returns a randomly
   selected integer uniformly distributed in the range  $[a, b]$ .
3:    $(\psi, \psi', \mathbf{E}, \mathbf{l}) := \text{QI\_SEARCH}(N, \phi_1, J, K, I, \mathbf{n}, \mathcal{I})$ 
4:   for  $i = 2$  to  $L$  do
5:      $(\psi_0, \psi'_0, \mathbf{E}_0, \mathbf{l}_0) := \text{QI\_SEARCH}(N, \phi_i, J, K, I, \mathbf{n}, \mathcal{I})$ 
6:     for  $j = 1$  to  $K + 1$  do
7:        $(p, f) := \text{BINARY\_SEARCH}(\psi'_{0,j}, \psi', K)$ 
8:       if  $f = \text{False}$  then
9:          $(\psi, \psi', \mathbf{E}, \mathbf{l}) := \text{UPDATE\_LIST\_SUB}(\psi'_{0,j}, \mathbf{E}_{0,j},$ 
            $\mathbf{l}_{0,j}, p, \psi, \psi', \mathbf{E}, \mathbf{l}, K)$ 
10:      end if
11:    end for
12:  end for
13: end function

```

and thus it is negligible because we consider the case for $K \ll 2^N$. Therefore, the reading order of the computational cost per an iteration with the system size N is $O(N^{J+1})$. The total computational cost in Algorithm 4 is thus $O(LIN^{J+1})$. In this study, we set the parameters as $(K, I, L) = (K_0, K_0, 1)$ and $(K, I, L) = (K_0, N, N)$ with $K_0 = N(N+1)/2 + 1$, and hence the total computational cost in both cases is $O(N^5)$.

IV. NUMERICAL RESULTS

Here, the QI multi search method is implemented to find the 120 lowest-energy states of the classical Ising model described by the Hamiltonian \hat{H}_0 in Eq. (1) with the system size N up to 30 sites. To analyze the efficiency of the QI research algorithm proposed here, we generate 120 different instances of the random coupling realizations in \hat{H}_0 for each system size N , which are treated exactly using the brute-force search in Sec. II.

A. Numerical setup and elapsed time

We investigate the elapsed time for the QI search method of Algorithm 4 with the following input parameters: $L = 1$ (i.e., equivalent to the QI single search method of Algorithm 3), $|\phi_1 = 0\rangle \equiv |00 \dots 0\rangle$ for the initial classical state, and $K = I = \sum_j n_j + 1$ with $\sum_j n_j = N + N(N-1)/2 = N(N+1)/2$, where we assume the infinitesimal quantum Hamiltonian

$$\hat{H}_1 = \epsilon \left(\sum_{i < j} \hat{\sigma}_i^x \hat{\sigma}_j^x + \sum_i \hat{\sigma}_i^x \right) \quad (4)$$

with the Pauli- X operator $\hat{\sigma}_i^x$ at the i th site and an infinitesimally small real number ϵ . Note that the one- and

two-spin flip operations considered in \hat{H}_1 correspond to the example for \mathbf{I}_1 and \mathbf{I}_2 , respectively, given in Sec. III.

According to the discussion toward the end of Sec. III, we expect that the leading order of the computational cost of the QI search with these inputs is $O(LIN^{J+1}) = O(N^5)$, which clearly has better scalability as compared to $O(2^N)$ for the brute-force search. To confirm the scalability, we perform the QI search on the HOKUSAI Big-Waterfall (CPU: Intel Xeon Gold 6148 2.4GHz) installed at RIKEN for the same sets of Hamiltonian \hat{H}_0 treated in Sec. II and estimate the averaged elapsed time without any parallelizations. As shown in Fig. 3, the elapsed time t of the QI search is nicely on the line of $t \sim N^5$ and becomes faster than that of the brute-force search for $N \geq 14$.

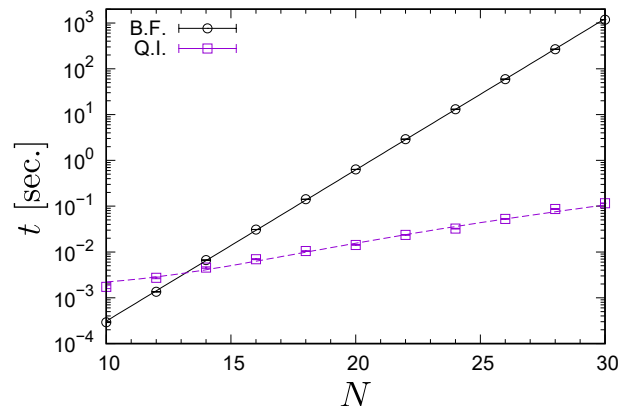


FIG. 3. (Color online) Averaged elapsed time t for the brute-force (BF) search and the quantum-inspired (QI) search with $L = 1$, $K = I = N(N+1)/2 + 1$, $J = 2$, $n_1 = N$, and $n_2 = N(N-1)/2$ as a function of the system size N . The black solid line and the purple dashed curve are fitting functions $\ln t = a_1 N + b_1$ with $(a_1, b_1) = (0.76, -15.7)$ and $t = a_2 N^5 + b_2$ with $(a_2, b_2) = (4.7 \times 10^{-9}, 1.8 \times 10^{-4})$, respectively.

B. N , L , and K dependence of the success probability for searching the ground state

Next, as the basic performance of the QI search algorithm, we investigate the N , L , and K dependence of the success probability p_1 for searching the ground state of the classical Ising Hamiltonian \hat{H}_0 , where p_1 is defined as the ratio between the number of instances of the random coupling realizations in \hat{H}_0 for which the ground state is correctly searched and the total number of instances of the random coupling realizations in \hat{H}_0 , which is 120 for each system size N in this study.

First, we perform the QI search by setting the parameters $(L, \phi_1) = (1, 0)$ and $I = K$ for the system sizes up to 30 sites. The number of lowest-energy states kept is set to be $K = aK_0$ with $a \in \{1, 2, 3, 10, 100\}$ and $K_0 = N(N+1)/2 + 1$. We can naively expect that p_1 decays exponentially with increasing N for a fixed value of a because the number of classical states generated in

the QI search for this setting is only $O(IN^2) \sim O(N^4)$, which is extremely smaller than the dimension 2^N of the total Hilbert space. However, as shown in Fig. 4, the probability p_1 decays slowly instead of exponentially for each value of a , and rapidly increases to close to 1 with increasing a . These characteristics are a supporting evidence of the high scalability of the QI search method.

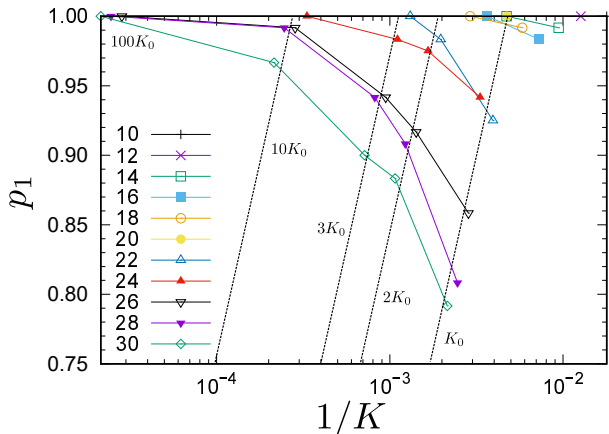


FIG. 4. (Color online) Success probability p_1 of the QI search with $(L, \phi_1) = (1, 0)$ and $I = K$ for different system sizes $N = 10, 12, \dots, 30$ indicated in the figure. The dotted lines are guide for the eye to highlight the slow decay of the success probability p_1 with increasing N for each $K \in \{K_0, 2K_0, 3K_0, 10K_0, 100K_0\}$ with $K_0 = N(N+1)/2+1$.

Second, we discuss the efficiency of the multi search with $L > 1$, where we introduce another set of the input parameters for the QI search: $L = N = 30$, $K = K_0$, and $I \in \{0.1N, 0.2N, 0.3N, 0.5N\}$. The 30 initial classical states are given randomly. The success probability p_1 as functions of the averaged elapsed time t is shown in Fig. 5. For comparison, the results shown in Fig. 4 for $N = 30$ are also plotted. Note that in Fig. 4 we set $L = 1$ but $I \sim O(N^2)$, and here we set $L = N$ but $I \sim O(N)$. Therefore, the overall computational complexity is $O(N^5)$ in both cases. Comparing the results of these two cases, we find that the averaged elapsed time t for the case of $L = N$ is always smaller than that for the case of $L = 1$ to achieve a given success probability p_1 . Surprisingly, all the ground states for the 120 different instances of the random coupling realizations in \hat{H}_0 for $N = 30$ can be correctly searched by the QI search algorithm with $(I, K, L) = (0.5N, K_0, N)$. This implies that if we parallelize the QI search for the different initial states with $L = N$, the computational speed can be $O(N)$ times faster. This is expected to be compatible with large-scale calculations using supercomputers for large system sizes.

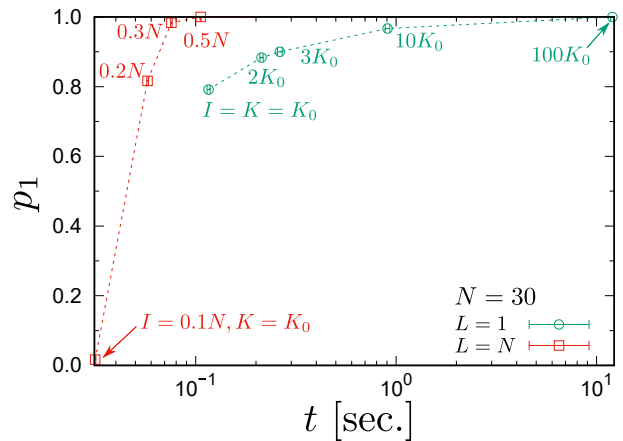


FIG. 5. (Color online) Success probability p_1 versus the averaged elapsed time t for searching the ground states of the 120 different instances of the random coupling realizations in \hat{H}_0 with $N = 30$. The QI multi search method with $L = N$, $K = K_0$, and $I \in \{0.1N, 0.2N, 0.3N, 0.5N\}$ is employed. For comparison, the results for the QI single search method with $L = 1$, $I = K$, and $K \in \{K_0, 2K_0, 3K_0, 10K_0, 100K_0\}$ are also shown by green circles. Here, $K_0 = N(N+1)/2+1$. Note that the computational complexity for these two methods with these parameters is $O(N^5)$.

C. Instance and initial state dependences of the number of iterations required for searching the ground state

To understand the reason why the QI multi search method with $L > 1$ improves the success probability p_1 , we now focus on the instance and initial state dependences of the number I_1 of iterations necessary to search the ground state of \hat{H}_0 . First, we employ the QI single search method with the parameters $(L, \phi_1) = (1, 0)$ and $I = K$ for K up to $K = 100K_0$. Figure 6(a) shows the results of I_1 for the 120 different instances of the random coupling realizations in \hat{H}_0 with different system sizes N , where the instance number is reordered so that I_1 monotonically increases. Then, we find that I_1 basically increases with the system size N .

To capture a feature of this increase, we show in Fig. 6(b) the ensemble-averaged I_1 , named I_a , and the median of the ensemble-dependent I_1 , named I_m , as a function of N . We find in Fig. 6(b) that $I_a > I_m$ for all the system sizes N . This is simply because I_1 's around instance #120 shown in Fig. 6(a) are especially large compared to those for other instances. According to the results in Fig. 4, I_a and I_m do not seem to increase exponentially with N . Therefore, as shown in Fig. 6(b), we fit I_a and I_m with power law functions and find that the exponent of N for I_m is smaller than that for I_a . This fitting also implies that the ground states of the half of the instances (i.e., Hamiltonian with different random coupling realizations) for the system size N can be searched successfully with the number of iterations up to only $I_1 \sim O(N^{2.3})$. Having obtained the different ex-

ponents, we speculate that the QI single search for the Hamiltonian \hat{H}_0 with the random coupling realizations around sample #120 is trapped in a local minimum since we employ the single initial state $|\phi_1 = 0\rangle \equiv |00\dots 0\rangle$.

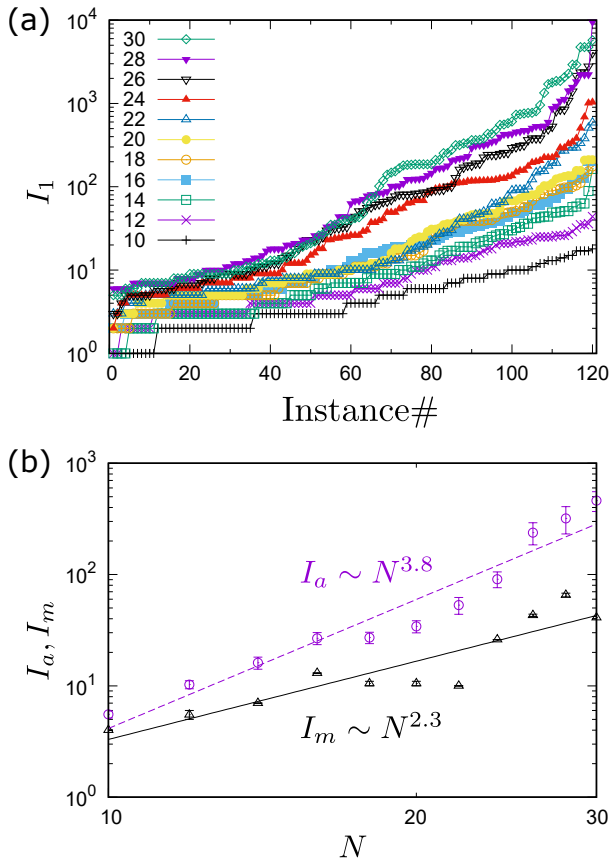


FIG. 6. (Color online) (a) Instance dependence of the number I_1 of iterations required to search the ground state of the classical Hamiltonian \hat{H}_0 for 120 different instances of the random coupling realizations with the system size $N = 10, 12, \dots, 30$ indicated in the figure. Note that the instance number is ordered so that I_1 monotonically increases for each N . (b) Ensemble-averaged I_1 (named I_a) and the median of the ensemble-dependent I_1 (named I_m) as a function of the system size N . The solid and dashed lines are power law fittings of I_m and I_a , respectively.

To confirm this assertion, we next explore the initial state dependence of I_1 by performing the QI multi search with $L = 120$ for the Hamiltonian \hat{H}_0 of instance #120 in Fig. 6(a). Figure 7 shows the results of I_1 as a function of the initial number for specifying the $L = 120$ different initial states that is ordered so that I_1 increases monotonically. We find that there are about 40 % of the initial states for which the ground state can be searched successfully by the QI search with only $I_1 < N$. This indicates that the multi search with $L > 1$ is an effective strategy to avoid trapping local minima.

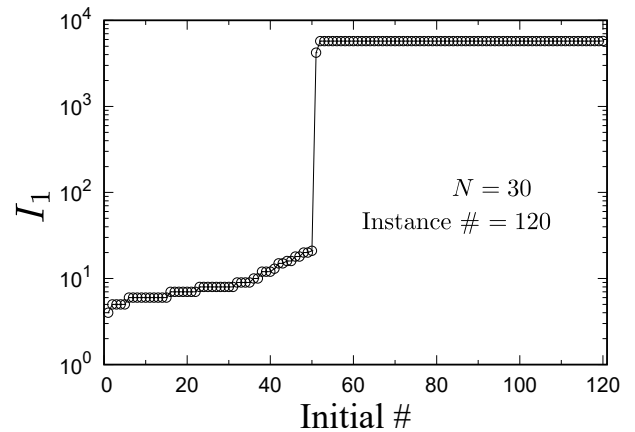


FIG. 7. Initial state dependence of the number I_1 of iterations. The Hamiltonian \hat{H}_0 is selected for the random coupling realization of instance # 120 in Fig. 6(a) with the system size $N = 30$. The QI multi search method is employed with $L = 120$ and the initial number for specifying the different initial states is ordered so that I_1 increases monotonically.

D. Search efficiency for low-energy states

Finally, we investigate the search efficiency of the QI search for the low-energy excited states of the classical Ising model described by the Hamiltonian \hat{H}_0 in Eq. (1). Note that when we perform the QI single search for obtaining the results shown in Fig. 4, K lowest-energy states, in addition to the ground state, are also kept. This is an advantage of the QI search algorithm proposed in this study. Here, we focus on 120 lowest-energy states and evaluate the ensemble-averaged success ratio r , defined as (the number of states that are successfully searched for a given random coupling realization in \hat{H}_0)/120 (i.e., the number of lowest-energy states that are aimed to search), which are averaged over the 120 different instances of the random coupling realizations in \hat{H}_0 . Figure 8 shows the results obtained by the QI single search with the parameters $(L, \phi_1) = (1, 0)$, $I = K = aK_0$, and $a \in \{1, 2, 3, 10, 100\}$ for the system sizes N up to 30 sites. Surprisingly, the K dependence of r is very similar to that of the success probability p_1 for search the ground state shown in Fig. 4. This implies that the QI single search algorithm shown in Algorithm 3 is highly scalable not only for the detection of the ground state but also for the search of low-energy excited states.

Figure 9 shows the success ratio r versus the averaged elapsed time t obtained by the QI single search method with $(L, K, I) = (1, aK_0, aK_0)$ and the QI multi search method with $(L, K, I) = (N, aK_0, aN)$ for the system size $N = 30$. Note that the overall computational complexity for these two methods with these parameters is both $O(N^5)$. We find in Fig. 9 that the success ratio r for the QI multi search method with $L = N$ is always better than that for the QI single search method with $L = 1$, assuming that the same averaged elapsed time t is taken. For example, comparing the results with $a = 2$

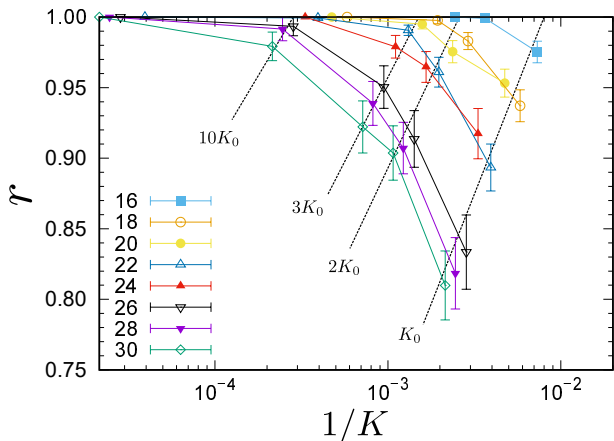


FIG. 8. (Color online) Success ratio r of the number of low-energy states successfully detected among 120 lowest-energy states for a given random coupling realization, which are averaged over the 120 different instances of the random coupling realizations in \hat{H}_0 , with different system sizes $N = 16, 18, \dots, 30$ indicated in the figure. The QI single search is employed with the parameters $(L, \phi_1) = (1, 0)$ and $I = K$. The dotted lines are guide for the eye to highlight the slow decay of the success ratio r with increasing N for each $K \in \{K_0, 2K_0, 3K_0, 10K_0, 100K_0\}$ with $K_0 = N(N+1)/2+1$.

for the QI single search method and r with $a = 1$ in the QI multi search method, which cost comparable elapsed time $t \sim 0.2$ seconds, the error $\epsilon = 1 - r$ of the search in the latter is about 8.3 times smaller than that in the former. We should also emphasize that the QI multi search method with $I = N$ can search already about 99% of the 120 lowest-energy states and the success rate r becomes even better with larger I . Thus, the QI multi search with $L > 1$ can search not only the ground state but also the low-energy states efficiently.

V. SUMMARY AND DISCUSSION

We have developed a quantum-inspired search algorithm for searching low-energy states of the classical Ising model described by the Hamiltonian \hat{H}_0 in Eq. (1) with the random Ising interactions J_{ij} and local magnetic fields h_i , to which the combinatorial optimization (NP) problems can be mapped. An essential point of our algorithm is to introduce infinitesimal quantum interactions \hat{H}_1 as in the quantum annealing, and generate and truncate direct product states inspired by the Krylov subspace method [20], a powerful method in the numerical linear algebra to calculate the eigenstates of a matrix with the smallest eigenvalues.

We have first investigated the low-energy properties of the Hamiltonian \hat{H}_0 by using the brute-force numerical search over all spin configurations for the system sizes up to $N = 30$ sites. Taking the ensemble average over the results for the 120 instances of the random coupling realizations in \hat{H}_0 , $\{J_{ij}, h_i\}$ being uniformly distributed in the

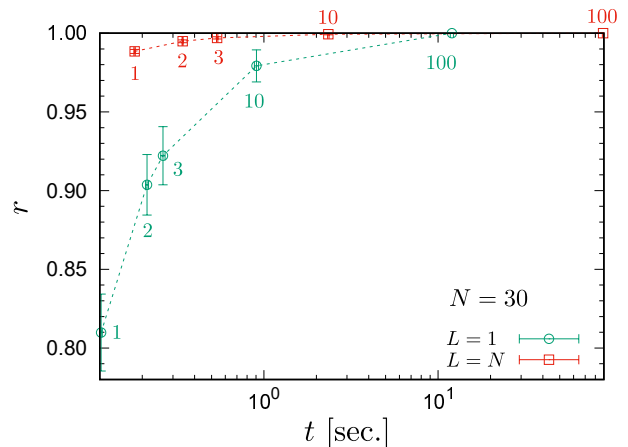


FIG. 9. (Color online) Success ratio r versus the averaged elapsed time t for searching 120 lowest-energy states of \hat{H}_0 with the system size $N = 30$. r and t are averaged over the 120 different instances of the random coupling realizations in \hat{H}_0 . The QI single search method with $(L, K, I) = (1, aK_0, aK_0)$ (denoted by green circles) and the QI multi search method with $(L, K, I) = (N, aK_0, aN)$ (denoted by red squares) are employed. Here, $a \in \{1, 2, 3, 10, 100\}$ and is indicated beside each symbol.

range of $[-1/2, 1/2]$, we have shown that the ensemble-averaged ground state energy E_1 scales as $N^{3/2}$ with the system size N , which is in good agreement with the case of the SK model, taking into account the fact that the coupling J_{ij} here is not scaled with N . We have also shown that there exists a finite energy gap between the ground state and the lowest excited state in the thermodynamic limit. Moreover, we have shown that the number of low-energy states increases exponentially with the excitation energy.

We have analyzed the performance of our QI search algorithm for the Hamiltonian \hat{H}_0 with the same 120 instances of the random coupling realizations used in the brute-force numerical search. We have shown that the QI multi search method (given in Algorithm 4) with $L = N$ random initial states can search the ground states successfully for all the 120 instances of the random coupling realizations with the system sizes up to $N = 30$ sites only by $I = N/2$ iterations. In addition, we have shown that 99% of the 120 lowest-energy states are successfully searched within $I = N$ iterations. The search accuracy is improved monotonically with increasing the number K of states kept and the number I of iterations. We have also shown that the QI search method is highly scalable with the system size N for the search of the ground state as well as the low-energy states. The overall computational complexity of the QI search method is $O(LIN^{J+1})$, and the algorithm can be easily parallelized with respect to L , thus compatible with the calculations for large systems using supercomputers.

Note that, our algorithm uses the bit operations and can easily treat the system sizes up to $N = 64$ by adopting 8-byte integers. However, the numerical cost for the

brute-force search is very expensive when $N > 30$, as it can be expected from Fig. 3. Therefore, to extend the study for the system sizes up to $N = 64$ sites, the MPI parallelization should be adopted, particularly for the brute-force search. Furthermore, we can adopt multi-byte integers or N -dimensional integer vectors to specify classical states when $N > 64$.

It is interesting to explore the search efficiency of the QI search considering as the infinitesimal quantum Hamiltonian \hat{H}_1 only the transverse magnetic field $\epsilon \sum_i \hat{\sigma}_i^x$ with $J = 1$ for the system sizes up to $N = O(1000)$. The computational cost with $J = 1$ is only $O(N^2)$ in each iteration, and thus it is comparable with the simulated annealing. However, since the number of classical states generated per an iteration is only $O(N)$, not $O(N^2)$ as in the case of $J = 2$ considered in this study, we can naively expect that the state list is much less updated in the QI search with $J = 1$, assuming that the number K of states kept is the same. As a consequence, the QI search with $J = 1$ may be easily trapped in local minima. Furthermore, the number I of iterations required to achieve the desired search accuracy may be increased in principle. Nonetheless, it is worthwhile to perform the QI search with $J = 1$ for the ground-state search of the system size as large as $O(1000)$ and compare the results obtained by other numerical methods such as the simulated annealing and the quantum annealing or by quantum devices such as D-Wave 2000Q system [27]. This is left for a future study.

In the classical Ising Hamiltonian \hat{H}_0 in Eq. (1), the total $\hat{\sigma}^z$ is a good quantum number. In order not to break this symmetry, we could introduce as the infinitesimal quantum interaction \hat{H}_1 the infinitesimal XX interaction $\epsilon \sum_{i < j} (\hat{\sigma}_i^x \hat{\sigma}_j^x + \hat{\sigma}_i^y \hat{\sigma}_j^y)$ by replacing the spin flip operations in Algorithm 1 with the spin exchange operations, and search the ground state and low-energy states for each sector of the total σ^z . Furthermore, the classical Hamiltonian \hat{H}_0 considered in statistical physics

and condensed-matter physics often has the translational and point group symmetries. We can also implement these symmetry constraints in the QI search algorithm by introducing a representative state for each sector with different quantum numbers associated with the symmetry [28], which is often used in the exact diagonalization method.

The QI search algorithm proposed here is inspired by the Krylov subspace method in that the infinitesimal quantum interactions \hat{H}_1 is considered to generate classical products states and truncate some of those states that have higher energies so that the fixed number of lowest energy states is kept. As we have demonstrated, after repeatedly applying this procedure, the ground state as well as the low-energy states of the classical Ising Hamiltonian \hat{H}_0 is successfully obtained. A similar algorithm might be applied to obtain the ground state of the quantum Hamiltonian $\hat{H} = \hat{H}_0 + \hat{H}_1$, where \hat{H}_0 is the classical Hamiltonian and \hat{H}_1 is the perturbatively small quantum Hamiltonian. It is a legitimate approximation in terms of perturbation theory to calculate the ground state by diagonalizing the Hamiltonian \hat{H} in the Hilbert space spanned by the finite number of classical products states, which are expanded by applying \hat{H}_1 and are then truncated according to their weights contributing the approximate ground state in the expanded Hilbert space.

ACKNOWLEDGMENTS

H.U. thanks T. Shirakawa and M. Ohzeki for helpful comments. The work was partially supported by KAKENHI No. 17K14359, and by JST PRESTO No. JPMJPR1911. This research used computational resources of the HOKUSAI BigWaterfall supercomputing system at RIKEN.

-
- [1] A. Lucas, *Frontiers in Physics* **2**, 5 (2014).
 - [2] F. Barahona, *J. Phys. A Math. Theor.* **15**, 3241 (1982).
 - [3] Y. Fu and P. W. Anderson, *Journal of Physics A: Mathematical and General* **19**, 1605 (1986).
 - [4] M. Mezard, G. Parisi, and M. Virasoro, *Spin Glass Theory and Beyond*, Lecture Notes in Physics Series (World Scientific, 1987).
 - [5] S. Kirkpatrick, C. D. Gelatt, and M. P. Vecchi, *Science* **220**, 671 (1983).
 - [6] T. Kadowaki and H. Nishimori, *Phys. Rev. E* **58**, 5355 (1998).
 - [7] E. Farhi, J. Goldstone, S. Gutmann, J. Lapan, A. Lundgren, and D. Preda, *Science* **292**, 472 (2001).
 - [8] S. Morita and H. Nishimori, *Journal of Mathematical Physics* **49**, 125210 (2008).
 - [9] A. Das and B. K. Chakrabarti, *Rev. Mod. Phys.* **80**, 1061 (2008).
 - [10] M. Ohzeki and H. Nishimori, *J. Comput. Theor. Nanosci.* **8**, 963 (2011).
 - [11] P. Ehrenfest, *Annalen der Physik* **356**, 327 (1916).
 - [12] M. Born and V. Fock, *Zeitschrift für Physik* **51**, 165 (1928).
 - [13] J. Schwinger, *Phys. Rev.* **51**, 648 (1937).
 - [14] T. Kato, *J. Phys. Soc. Jpn.* **5**, 435 (1950).
 - [15] Y. Seki and H. Nishimori, *Phys. Rev. E* **85**, 051112 (2012).
 - [16] Y. Susa, Y. Yamashiro, M. Yamamoto, and H. Nishimori, *J. Phys. Soc. Jpn.* **87**, 023002 (2018).
 - [17] A. M. Ferrenberg and R. H. Swendsen, *Phys. Rev. Lett.* **61**, 2635 (1988).
 - [18] A. M. Ferrenberg and R. H. Swendsen, *Phys. Rev. Lett.* **63**, 1658 (1989).
 - [19] F. Wang and D. P. Landau, *Phys. Rev. Lett.* **86**, 2050 (2001).
 - [20] Z. Strakoš and J. Liesen, *Krylov Subspace Methods Principles and Analysis*, Numerical Mathematics and Scientific Computation (Oxford university press, 2012).

- [21] D. Sherrington and S. Kirkpatrick, *Phys. Rev. Lett.* **35**, 1792 (1975).
- [22] M. Palassini and A. P. Young, *Phys. Rev. Lett.* **83**, 5126 (1999).
- [23] M. Palassini, *J. Stat. Mech. Theory Exp.* **2008**, P10005 (2008).
- [24] J.-P. Bouchaud, F. Krzakala, and O. C. Martin, *Phys. Rev. B* **68**, 224404 (2003).
- [25] S. Boettcher, *Phys. Rev. Lett.* **95**, 197205 (2005).
- [26] S.-Y. Kim, S. J. Lee, and J. Lee, *Phys. Rev. B* **76**, 184412 (2007).
- [27] “The D-Wave 2000Q™ System,” <https://www.dwavesys.com/d-wave-two-system>.
- [28] A. W. Sandvik, *AIP Conf. Proc.* **1297**, 135 (2010).